Optimization of Vortex Shedding in 3-D Wakes Using Belt Actuators

Philippe Poncet, Petros Koumoutsakos

Optimization of Vortex Shedding in 3D Wakes using Belt Actuators

Philippe Poncet
Laboratory Mathematics for Industry and Physics,
National Institute of Applied Sciences (INSA),
Toulouse, France

Petros Koumoutsakos
Institute of Computational Science,
Swiss Federal Institute of Technology
Zürich, Switzerland

ABSTRACT

This paper discusses the control of cylinder wakes via tangential wall velocity modifications. The wall velocity is piecewise constant (corresponding to belt actuators) and its amplitude is optimized using a clustering real coded Genetic Algorithm. This type of control significantly affects the vortical structures that are being shed in the wake and it is shown that the flow gets significantly modified resulting in a three dimensional body shedding two dimensional vortical structures.

KEY WORDS: Shedding manipulation; genetic algorithms; three-dimensional wakes; vortex methods; hydrodynamic instabilities.

INTRODUCTION

We are interested in the manipulation of vortex shedding of three-dimensional wakes and the associated drag reduction in the canonical case of a 3D cylinder. Control is performed by means of tangential velocities on the body, which in practice can be translated as wall parallel "belts-actuators" or tangential local jets. We develop suitable numerical methods to solve numerically the 3D Navier-Stokes equations and implement clustering genetic algorithms in order to optimize the actuator parameters.

In order to compute accurately these flows a Vortex-in-Cell method using a coupling between grids and particles is developed. Vortex methods make the non-linearity of the transport terms vanish from the Navier-Stokes equation, and thus alleviate the related stability condition usually encountered in Eulerian schemes that can be very restrictive on the time-step. This advantage of Lagrangian method is counterbalanced by a lack of accuracy, especially for Vortex methods based on random walks. The coupling between particles and grids permits to overcome this difficulty and in addition to reduce the computational cost of evaluating the velocity field (even when compared to multipoles methods for the Biot-Savart laws). The associated integrals and derivative operators can be computed with a good accuracy. This has been validated in Cottet and Koumoutsakos (2000), Cottet and Poncet (2002, 2003, 2004), Poncet (2002, 2004).

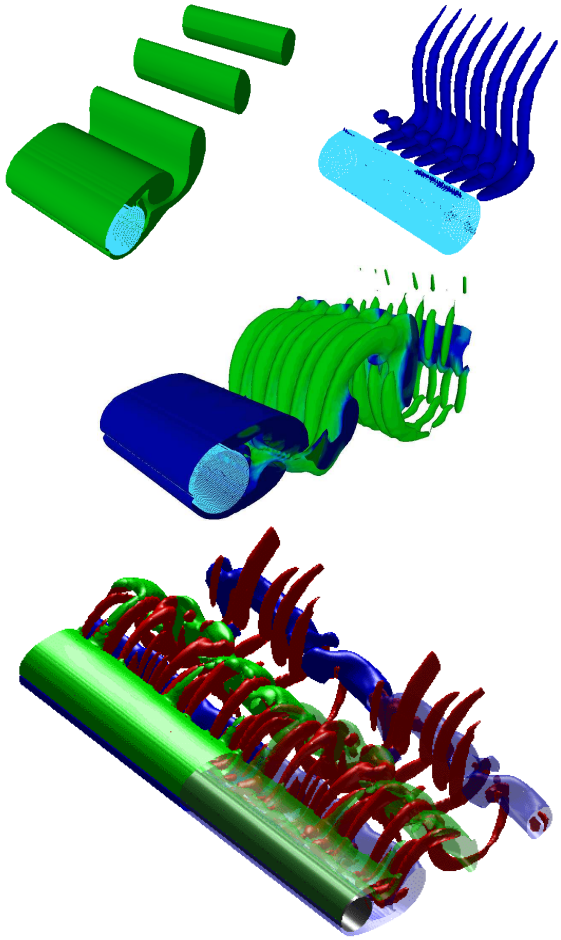

Fig. 1 : Dynamics of the cylinder wake in 3D at Re=300. Two-dimensional wake (above, to the left), first signature of instability (above, to the right), resultant 3D wake before saturation (middle) and post-transient established 3D flow with fully developed hydrodynamic instabilities (below, from Poncet (2004)).

In order to perform a control by means of a tangential wall velocity("belts" actuators), we first consider the two-dimensional problem. This has been obtained by Genetic Algorithm, whose histogram and most probable solution are provided in Milano and Koumoutsakos (2002) and in the present paper.

This two-dimensional profile of velocity is then fitted by a smooth symmetric function, and applied on three-dimensional flows (see Poncet, Cottet and Koumoutsakos, to appear in C. R. Mécanique). On these 3D simulations one can observe the behavior of three-dimensionality, the drag reduction and the shedding cancellation (in the sense of force oscillation, *ie* drag and mean vorticity variations). One can also check that the property of shedding reduction is still valid when a full 3D profile of velocity is applied on the body.

NUMERICAL APPROACH

We consider the three-dimensional Navier-Stokes equations in their velocity-vorticity formulation

$$\frac{\partial \omega}{\partial t} + u \cdot \nabla \omega - \omega \cdot \nabla u - \nu \Delta \omega = 0 \qquad (1)$$

where ω is the vorticity field, u the velocity field and ν the kinematic viscosity. This equation is defined over a cylindrical domain, around a cylinder of diameter D ($R=D/2$ will denote the radius) and spanwise length L. One considers L-periodic solutions. The far field condition on velocity is $U \to U_\infty e_x$ where e_x is the streamwise basis vector.

Moreover, the relation $\omega = \text{curl } u$ is satisfied for all time, as well as the incompressibility div $u = 0$ and the no-slip condition $u = 0$ on the body.

The Reynolds number $Re=U_\infty D/\nu$ gives an information on the flow nature (steady, oscillatory, 3D unstable, turbulent, …). In the present simulations, one has Re=300 for 3D simulations and 500 for 2D simulations.

The numerical method used to solve the Navier-Stokes equations (1) is an hybrid vortex method, joined to a time-splitting algorithm for convection and diffusion.
One considers the vorticity field in its lagrangian formulation

$$\omega(t) = \sum_{p=1}^{n} \omega_p(t) \delta_{x_p(t)} v_p \qquad (2)$$

where $\omega_p(t)$ is the particle vorticity, $x_p(t)$ is the characteristic curve and v_p the volume of the particle (which remains constant in time due to the incompressibility). The time-splitting algorithm is described below.

Lagrangian convection step

The convection part can thus be written :

$$\begin{cases} \dfrac{d\omega_p}{dt} = \omega \cdot \nabla u(x_p) \\ \dfrac{dx_p}{dt} = u(x_p) \\ \dfrac{dv_p}{dt} = v_p \operatorname{div} u(x_p) = 0 \end{cases} \qquad (3)$$

which is a standard dynamical system (of size 6n, n being the number of particles) whose stability is only limited by $\|\nabla u\|^{-1} \cong \|\omega\|^{-1}$.
Such a strong stability is very useful to perform accurate simulations for long time, and its lagrangian features gives a natural approach of transport since the transport part of the Navier-Stokes equations is implicitly solved (simplified by the introduction of the characteristic curves).

This dynamical system is numerically solved by a Runge-Kutta scheme of second or fourth order. The velocity and its gradient is computed by an hybrid technique :

- Vorticity carried by particle is interpolated on a grid, by means of a convolution based on a third order compact-supported kernel (Monaghan's M_4'),
- The stream is computed on this grid, by solving a Poisson equation (in the present case in cylindrical coordinates), satisfying the no-slip-through condition,
- The velocity, *ie* the stream curl, is computed on the grid, in practice with fourth order centered finite-difference scheme,
- The velocity gradient and its product with the vorticity (the stretching term) are computed on the grid,
- Stretching and velocity are finally interpolated back to particles. Equation (3) can then be advanced in time.

The details of this algorithm are fully developed in Cottet and Poncet (2003), and in its elementary formulation in Ould-Sahili, Cottet and El-Hamraoui (2000).

Diffusion step

The diffusion part is a heat equation on vorticity, defined on the cylindrical domain Ω, which reads

$$\begin{cases} \dfrac{\partial \omega}{\partial t} - \nu \Delta \omega = 0 \text{ on } \Omega \\ L(\omega) = f(\tilde{u}) \text{ on } \partial\Omega \\ \omega(0) = \tilde{\omega} \text{ on } \Omega \end{cases} \qquad (4)$$

The initial condition $\tilde{\omega}$ is the final vorticity of the convection step. The boundary condition $L(\omega) = f(\tilde{u})$ aims at canceling the residual slip $\tilde{u}$ obtained after the convection step. Function f is linear in $\tilde{u}$ and depends on time step and viscosity. Operator L is a tensorial differential operator of the vorticity and its flux on the body, developed in Cottet and Poncet (2003), and Poncet (2004)).

Equation (4) is itself decomposed by linearity in two parts :

$$\begin{cases} \dfrac{\partial \omega}{\partial t} - \nu \Delta \omega = 0 \text{ on } \Omega \\ L(\omega) = 0 \text{ on } \partial\Omega \\ \omega(0) = \tilde{\omega} \text{ on } \Omega \end{cases} \qquad (5)$$

solved by a Particle Strength Exchange lagrangian scheme (Degond and Mas-Gallic, 1989) in its discreet formulation, and

$$\begin{cases} \dfrac{\partial \omega}{\partial t} - \nu \Delta \omega = 0 \text{ on } \Omega \\ L(\omega) = f(\tilde{u}) \text{ on } \partial\Omega \\ \omega(0) = 0 \text{ on } \Omega \end{cases} \quad (6)$$

whose solution is expressed under its integral form. The solution of this last equation has its significant values close to the body, and is actually the viscous effect creating the boundary layer (see Cottet and Poncet, 2003 for further details).

Validation

This method and its immersed-boundary variant have been validated on numerous test cases in its early developments, including ring-vortex wall interaction (Cottet and Koumoutsakos, 2000), 2D wakes (Cottet and Poncet, 2002). The annular vortex and 3D cylinder interaction involves the ring propulsion, curved boundary layer and fusion between the main ring and the boundary layer, generating a secondary ring (Cottet and Poncet, 2003; Fig. 2).

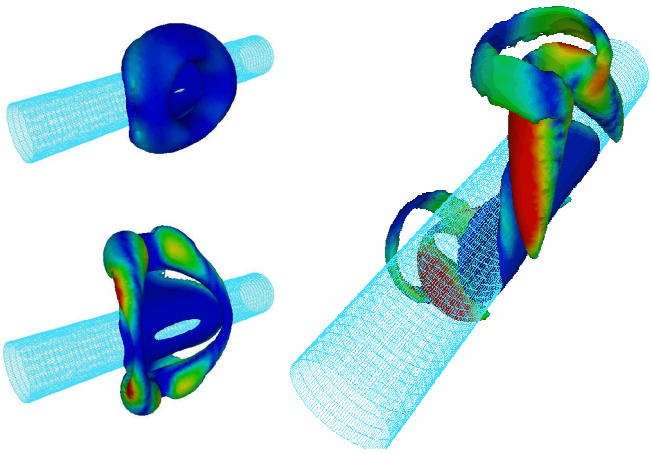

Fig. 2 : Annular vortex and cylinder interaction, fusion between main ring and boundary layer, generating a secondary ring-vortex (snapshots of vorticity at three different times).

The main field of application of this numerical method was the computation of three-dimensional cylinder wakes, whose validation was mainly based on Williamson (1996) and Barkley and Henderson (1996) results. One can recover the main diagnostics for Reynolds numbers between 100 and 800, such as drag coefficient, Strouhal number (non-dimensional frequency), 3D instability wavelength and spectral profile (Cottet and Poncet 2003; Poncet and Cottet, 2003; Poncet 2004; Fig. 1). One can also recover drag curves of impulsively started cylinder in 2D up to *Re*=9500 in the early development of the wake (Cottet and Poncet, 2002). Some topological aspects of wakes behind cylinder into rotationally oscillations have also been shown (Poncet, 2002). The typical drag and lift coefficients for a unstable cylinder wake at Re=300 are plotted on figure 3.

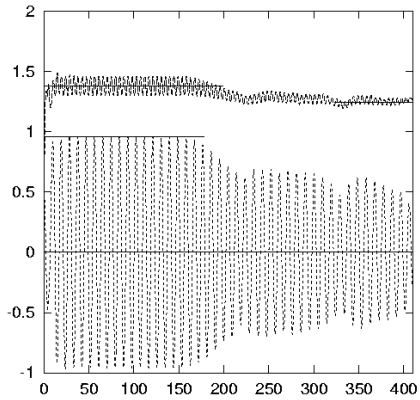

Fig. 3 : Typical drag (—) and lift (- - -) coefficient of a cylinder wake developing streamwise hydrodynamic instabilities at Re=300.

OPTIMIZATION PROCESS

In order to obtain a velocity profile on the body useful for 3D control, it is wise in a first approach to get a two-dimensional profile from 2D simulations. The algorithm presented herein aims at optimizing the drag reduction.

Control of 2D flows

One thus considers a 2D cylinder with 16 equally long panels on the body, segments numbered from 1 to 16 (see figure 4). Velocity profiles are thus elements in $]-b, b[^{16}$, the range b being the maximum velocity allowed. This leads to an optimization problem in a control space of dimension 16, with a non-linear cost function, whose shape is basically unknown. Genetic Algorithms consequently seems a good approach in order to get close to the optimal solution.

A population of profiles in generated and each element of the population is associated to a score based on drag reduction. Then a mutation process builds a new population whose each element requires a flow computation running until an established regime is reached in order to associate a score.

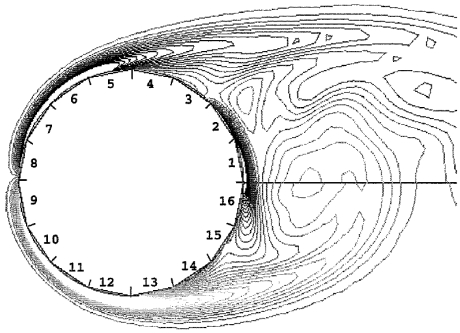

Fig. 4 : Panel setup and flow example resulting from a belt actuators configuration.

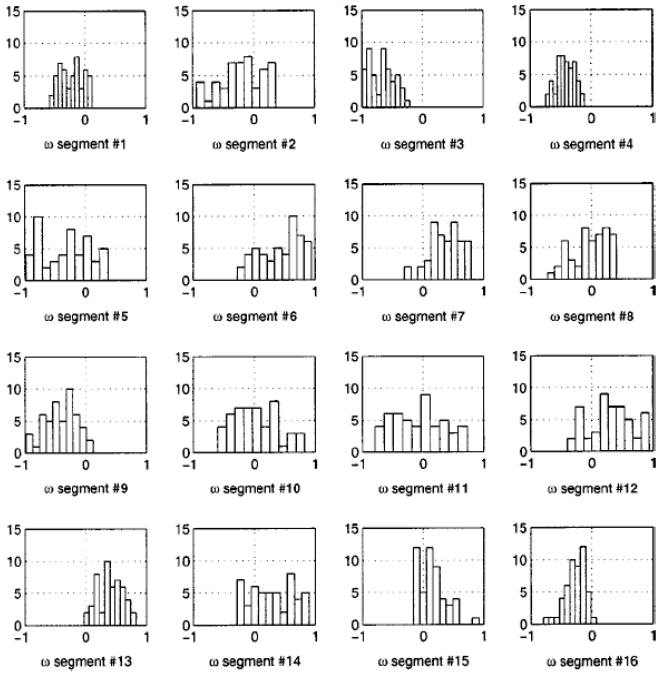

Fig. 5 : Histogram of population: number of occurrences with respect to velocity values for each segment 1-16 (see figure 4).

Histograms plotted on figure 5 have been obtained by the Genetic Algorithm described in Milano and Koumoutsakos (2002), itself based upon the 2D Navier-Stokes solver on a stretched O-grid by Mittal (1995). An example of the resultant flow and drag coefficient are given on figures 4 and 6.

On figure 6 is also plotted (dashed line) the drag coefficient resulting from an optimization using only the four most significant actuators of the global optimization process, in the present case the actuators 3, 4, 13 and 14. This technique is called Clustering Genetic Algorithm (usually abbreviated by "CGA", from Milano and Koumoutsakos, 2002), and provides an important gain of energy with only a minimal loss of drag reduction, thus a gain of efficiency.

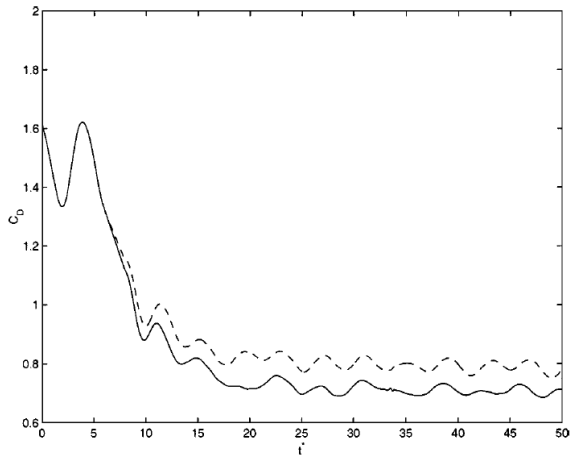

Fig. 6 : Resulting drag coefficient for the best populations, using all actuators (—) and only the four most significant actuators (clustering technique, - - -).

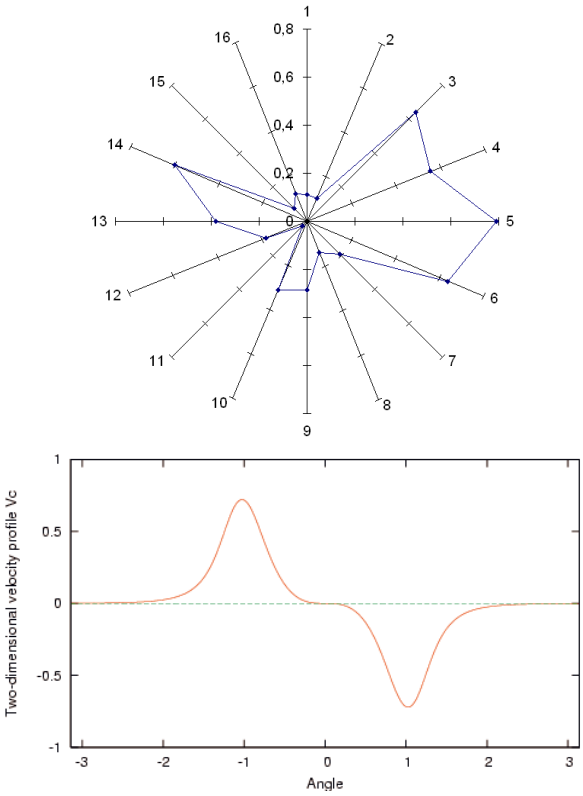

Fig 7 : Most probable velocity profile obtained with the genetic algorithm (■) (above, absolute velocity with respect to segment number), and plot of the fitting continuous smooth function $f(\theta)$ from formula (7) (below, velocity versus angle).

Control of 3D flows

In order to apply this two-dimensional result to three-dimensional simulations, one needs to use a smooth symmetric function fitting the most probable distribution of velocity obtained by the GA and CGA. Indeed, all the elements of profile population are zero mean value (and consequently the best population), but not necessarily the most probable, which is only the distribution of highest values on the histogram. The property of zero-circulation (to avoid the drag changed into lift) is required and thus the symmetry of the smooth velocity distribution. Moreover, the main values of the clustered population have been used to get the smooth profile (whose some significant values are plotted on figure 6), given in Cottet and Poncet (2004) by :

$$f(\theta) = -\sin\left(\frac{3.2\theta^3}{3+\theta^{10}}\right) \qquad (7)$$

with $\theta \in]-\pi, \pi[$.

The tangential velocity profile is then given by

$$V_{slip}(\theta) = C\, f(\theta) \qquad (8)$$

where C is a coefficient (equal to 1 for the fitting profile, see figure 7) to tune the energy level involved in the control.

This smooth profile is then applied to a 3D flow for a Reynolds number

Re=300, with streamwise hydrodynamic instabilities fully developed. In order to quantify the flow shedding, a interesting quantity is the total spanwise vorticity in a neighborhood of the body (basically the sum of the von Kármán alleys, *ie* eddies aligned with the cylinder axis), given by

$$\Gamma_z(t) = \int_{\Omega} \omega_z(x, y, z, t)\, \mathrm{d}\, v \qquad (9)$$

The effect of the 2D smooth velocity profile on the global spanwise vorticity of the 3D flow, with $C=1$, is plotted on figure 9, and snapshots of the 3D iso-vorticity levels are given on figure 8. One can see that the shedding vanishes almost completely in the neighborhood of the body.

Moreover, since the residual shedding occurs far from the body, it does not affect the boundary layer anymore, thus also a cancellation of oscillations in the drag forces (resulting drag coefficient is plotted on figure 10).

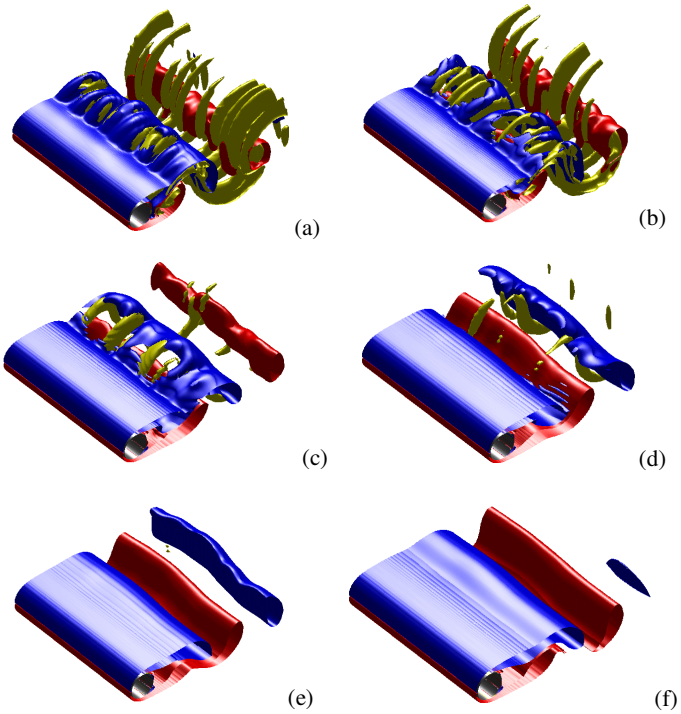

Fig. 8: Isovalues of vorticity after control activation with smooth velocity profile, at different times ((a) to (f) respectively at t=270, 280, 290, 300, 310 and 320), from Cottet and Poncet (2004).

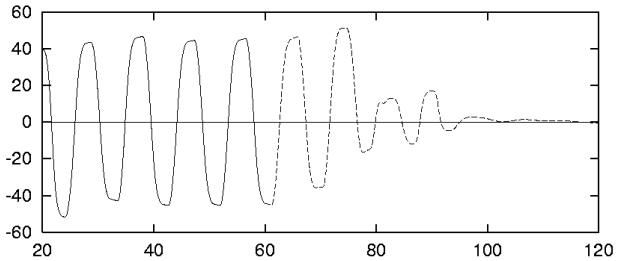

Fig. 9 : Shedding (mean spanwise vorticity) before and after control activation (at t=60) for a 2D control of 3D flow.

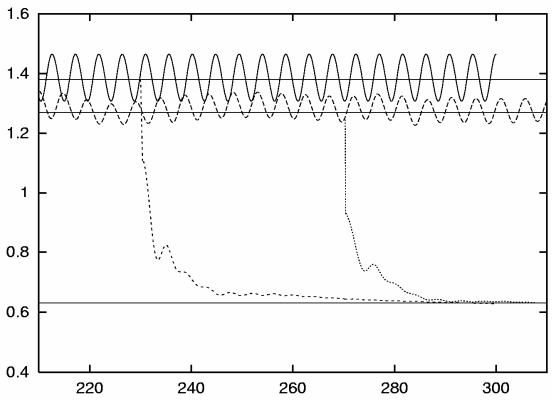

Fig. 10 : Drag reduction and drag oscillation cancellation for 2D flows (— uncontrolled, - - - controlled, activation at t=230) and 3D flows (– – uncontrolled, · · · · controlled, activated at t=270).

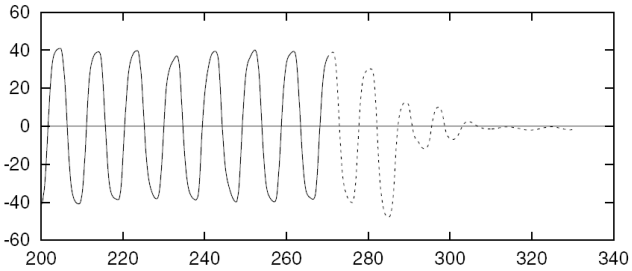

Fig. 11 : Shedding (mean spanwise vorticity) before and after control activation (at t=270) for a 3D control of 3D flow.

Another interesting property of applying tangential velocity is that the shedding reduction does not depend on the fact that the profile is 2D or not. Indeed, when one modifies the profile into

$$V_{slip}(\theta, z) = \frac{2C}{\sqrt{5}}(1+\sin z)\, f(\theta) \qquad (10)$$

then the shedding also vanishes almost completely (see figure 11), here with a full three-dimensional profile (z being the spanwise component). This last 3D profile uses the same energy as the previous 2D profile given by formula (8), hence a fair comparison between the two results.

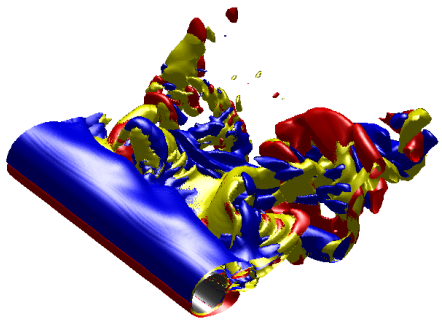

Fig. 12 : Effect of 3D control of 3D flow at large energies and large wavelength (locked on mode A).

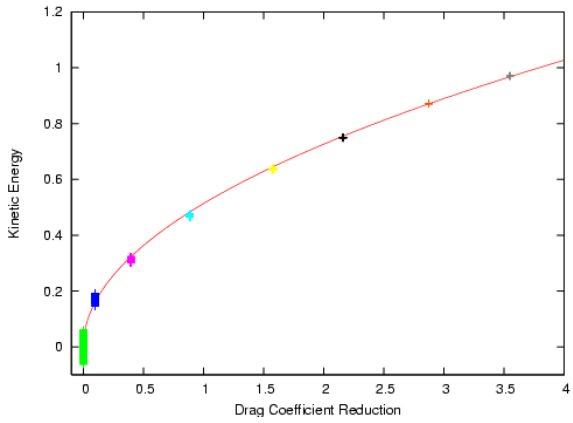

Fig. 13 : Drag coefficient reduction versus kinetic energy, for various values of C (left to right : 0, 0.25, 0.5, 0.75, 1, 1.17, 1.35, and 1.5), and its square-root regression.

DEPENDENCY OF DRAG OSCILLATION VERSUS ENERGY

In the last section, the tangential velocity profile given formula (8) has led, in the case *C=1*, to a substantial reduction of shedding in the sense of the spanwise vorticity integral in the body neighborhood (figure 10), accompanied by a large drop of the drag coefficient (figure 9), that is to say a large difference between controlled and uncontrolled drag coefficients. The reference is the drag coefficient of the three-dimensional uncontrolled flow, 1.262 from Cottet and Poncet (2003). Moreover, one can notice that large energies may lead to a complete loss of the von Kármán eddies structuring the uncontrolled flow (see figure 12).

Since the drag and lift forces are given by the drag and lift coefficients, a study of oscillations of these quantities, especially the drag coefficient, would clarify how the shedding reduction is linked to the energy involved in the control. Formula (8) implies

$$E_c = \int_\Omega V_{slip}(\theta)^2 \, d\theta = C^2 \int_\Omega f(\theta)^2 \, d\theta \qquad (11)$$

thus kinetic energy involved to enforce the velocities on body behaves as C^2. It has been noticed in the past that the pressure part of the drag coefficient is a linear function of the radial derivative of vorticity (Cottet and Koumoutsakos, 2002; Cottet and Poncet, 2003), itself a linear function of the residual velocity at the end of the convection step given by formula (3). This spurious velocity is in practice a fraction of the velocity imposed on boundary.

Consequently, one can expect a linear behavior between the drop of drag coefficient and the boundary velocity amplitude *C*.. Moreover, the kinetic energy is quadratic in *C*, by means of formula (11). It is thus highly expected to observe a square-root regression of the drop of mean drag coefficient with respect to the kinetic energy involved in the control. This fact is indeed observed and plotted on figures 13 and 14, in standard and logarithmic scales, for various values of *C*.

Once the behavior of drag reduction with respect is identified, it is thus possible to study the deviation of the drag coefficient (force oscillation) from its mean value. For small energies, this deviation is plotted of figure 15, on which the oscillation follows seemingly an inverse polynomial law for energies lesser than 1 :

$$Max\left|\Delta C_D\right| \cong 0.033\left(1+4.5\,E_c\right)^{-1} \qquad (12)$$

For larger energies (up to 4, see figure 16), one observes a slower decreasing property :

$$Max\left|\Delta C_D\right| \cong 0.06\left(1+13\,E_c\right)^{-0.9} \qquad (13)$$

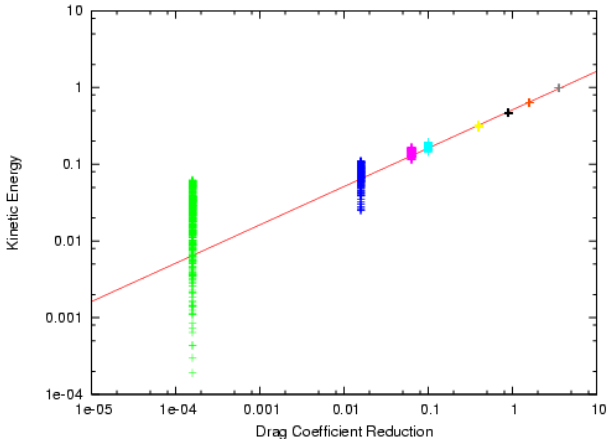

Fig. 14 : Drag coefficient reduction versus kinetic energy in logarithmic scale, for various values of C (left to right : 0.01, 0.1, 0.2, 0.25, 0.5, 0.75, 1, and 1.5), and its square-root regression.

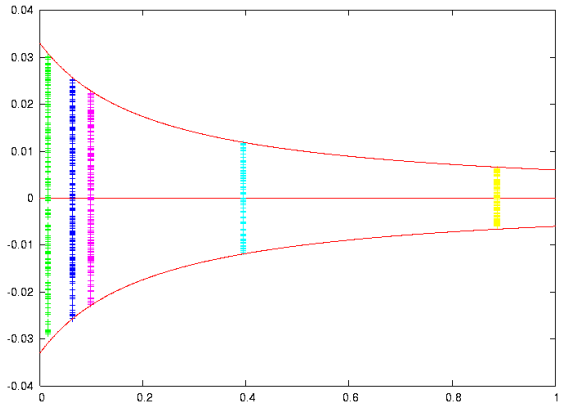

Fig 15 : Shedding reduction : drag coefficient (deviation from mean value) versus kinetic energy in low-energy control (small values of C), and its fitting curve.

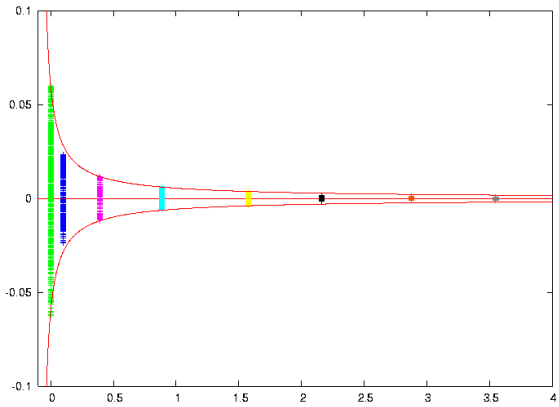

Fig 16 : Same as figure 15 for larger values of C.

Nevertheless, for both the cases, the oscillation amplitude is roughly proportional to the inverse of kinetic energy involved in the control. Furthermore, one can also check that the drag oscillation is a good

representative of force oscillation. Indeed, as shown on figures 17 and 18, the lift oscillations decrease as the drag no longer oscillates.

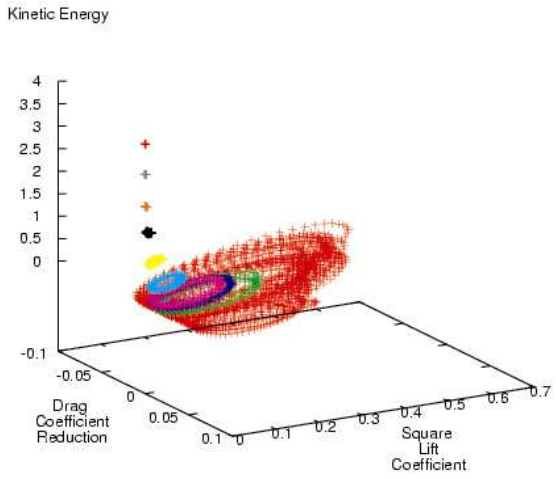

Fig 17 : Attractor : Drag coefficient / Lift coefficient / Energy (formula 11).

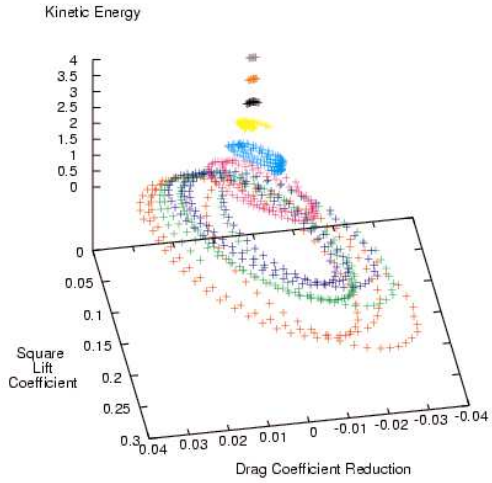

Fig 18 : Same as figure 17 without uncontrolled data.

CONCLUSION

A clustering genetic algorithm has been used to build a quasi-optimal two-dimensional profile of tangential velocities on a cylindrical body. The optimality is in the sense of the drag coefficient optimization.

This profile is then applied to a three-dimensional flow in order to study the effect of such a control on three-dimensionality and realistic drag coefficient. In order to avoid a lack of regularity (and thus a lack of accuracy), the profile obtained by the genetic algorithm is smoothed. The flow is computed by a robust vortex-in-cell method in order to reach long time scales, computed over a large domain, with small wavelength instabilities to compute accurately.
These simulations have shown that the mean drag coefficient behaves as a square-root function of the energy involved in the control, and the force oscillations (shedding) decrease as the inverse of energy.

An other quantity measuring the shedding is the amount of spanwise vorticity in the body neighborhood. This quantity is intrinsic to the flow and is not related to forces, but gives a good idea of how the flow oscillates. It exhibits a sharp drop when control is activated, and shows that shedding almost completely vanish. The same behavior has been observed when control is fully three-dimensional, which means that the shedding reduction may not depend on the spanwise-constant property of the tangential velocity profile, but only on the energy involved, at least for large energies.

Tangential actuators, such as the model belt actuators proposed herein, offer the advantage that when inactive they do not add to the drag of the system. The incorporation of such actuators in engineering systems can offer a multitude of synergetic control possibilities, through their spatial arrangement and the time dependence and schedule of their activation.

ACKNOWLEDGEMENTS

The authors would like to thank Pr Georges-Henri Cottet for his participation during the development of this work. We also would acknowledge the computational support of CEA-CENG (Grenoble, France).

REFERENCES

Barkley, D, and Henderson, R D (1996). “Three dimensional Floquet stability analysis of the wake of a circular cylinder,” *J. Fluid Mech*., Vol 332, pp 215-241.

Cottet, G-H, and Koumoutsakos, P (2000). *Vortex Methods, Theory and Practice*, Cambridge University Press.

Cottet, G-H, and Poncet, P (2004). “New results in the simulation and control of three-dimensional cylinder wakes,” Comput. Fluids, Vol 33, pp 697-713.

Cottet, G-H, and Poncet, P (2003). “Advances in Direct Numerical Simulations of three-dimensional wall-bounded flows by Vortex In Cell methods,” *J. Comp. Phys*., Vol 193, pp 136-158.

Cottet, G-H, and Poncet, P (2002). “Particle methods for direct numerical simulations of three-dimensional wakes,” *J. Turbulence*, Vol 3, No 38, pp 1-9.

Degond, P, and Mas-Gallic, S (1989). “The Weighted particle method for convection-diffusion equations,” *Math. Comput.,* Vol 53, pp 485-526.

Milano, M, and Koumoutsakos, P (2002). “A clustering genetic algorithm for cylinder drag optimization,” *J. Comp. Phys*., Vol 175, pp 79-107.

Mittal, R (1995). “Large-Eddy Simulation of Flow Past a Circular Cylinder,” Center for Turbulence Research, *Annual Research Briefs*, p 107.

Ould-Sahili, M L, Cottet, G-H, and El Hamraoui, M (2000). “Blending finite-differences and vortex methods for incompressible flow computations,” *SIAM J. Sci. Comput*., Vol 22, pp 1655-1674.

Poncet, P (2004). “Topological aspects of three-dimensional wakes behind rotary oscillating circular cylinders,” *J. Fluid Mech*., Vol 517, pp 27-53.

Poncet, P, and Cottet, G-H (2003). “Open-loop control of three-dimensional wakes,” *Proceedings of the Second MIT Conference,* Vol 2, pp 2348-2351.

Poncet, P (2002). “Vanishing of mode B in the wake behind a rotationally oscillating circular cylinder,” *Phys. Fluids*., Vol 14, No 6, pp 2021-2024.

Williamson, C H K (1996). “Three-dimensional wake behind a cylinder,” *J. Fluid Mech*., Vol 328, p 345.